Chapter 8

The Ekman Layer

(July 12, 2006) **SUMMARY**: Frictional forces, neglected in the previous chapter, are now investigated. Their main effect is to create horizontal boundary layers that support a flow transverse to the main flow of the fluid. The numerical treatment of the velocity profiles dominated by friction is illustrated with a spectral approach.

8.1 Shear turbulence

Because most geophysical fluid systems are much shallower than they are wide, their vertical confinement forces the flow to be primarily horizontal. Unavoidable in such a situation is friction between the main horizontal motion and the bottom boundary. Friction acts to reduce the velocity in the vicinity of the bottom, thus creating a vertical shear. Mathematically, if u is the velocity component in one of the horizontal directions and z the elevation above the bottom, then u is a function of z, at least for small z values. The function $u(z)$ is called the *velocity profile* and its derivative du/dz, the *velocity shear*.

Geophysical flows are invariably turbulent (high Reynolds number) and this greatly complicates the search for the velocity profile. As a consequence, much of what we know is derived from observations of actual flows, either in the laboratory or in nature.

The turbulent nature of the shear flow along a flat or rough surface includes variability at short time and length scales, and the best observational techniques for the detailed measurements of these have been developed for the laboratory rather than outdoor situations. Laboratory measurements of nonrotating turbulent flows along smooth straight surfaces have led to the conclusion that the velocity varies solely with the stress τ_b exerted against the bottom, the fluid molecular viscosity ν, the fluid density ρ and, of course, the distance z above the bottom. Thus,

$$u(z) \;=\; F(\tau_b, \nu, \rho, z).$$

Dimensional analysis permits the elimination of the mass dimension shared by τ_b and ρ but not present in u, ν and z, and we may write more simply:

217

$$u(z) \; = \; F\left(\frac{\tau_b}{\rho}, \nu, z\right).$$

The ratio τ_b/ρ has the same dimension as the square of a velocity, and for this reason it is customary to define

$$u_* \; = \; \sqrt{\frac{\tau_b}{\rho}} \,, \tag{8.1}$$

which is called the *friction velocity* or *turbulent velocity*. Physically, its value is related to the orbital velocity of the vortices that create the cross-flow exchange of particles and the momentum transfer.

The velocity structure thus obeys a relation of the form $u(z) \; = \; F(u_*, \nu, z)$ and further use of dimensional analysis reduces it to a function of a single variable:

$$\frac{u(z)}{u_*} \; = \; F\left(\frac{u_* z}{\nu}\right). \tag{8.2}$$

In the presence of rotation, the Coriolis parameter enters the formalism and the preceding function depends on two variables:

$$\frac{u(z)}{u_*} \; = \; F\left(\frac{u_* z}{\nu}, \frac{f z}{u_*}\right). \tag{8.3}$$

8.1.1   Logarithmic profile

The observational determination of the function F in the absence of rotation has been repeated countless times, yielding the same results every time, and it suffices here to provide a single report (Figure 8-1). When the velocity ratio u/u_* is plotted versus the logarithm of the dimensionless distance $u_* z/\nu$, not only do all the points coalesce onto a single curve, confirming that there is indeed no other variable to be invoked, but the curve also behaves as a straight line over a range of two orders of magnitude (from $u_* z/\nu$ between 10^1 and 10^3).

If the velocity is linearly dependent on the logarithm of the distance, then we can write for this portion of the velocity profile:

$$\frac{u(z)}{u_*} \; = \; A \, \ln \frac{u_* z}{\nu} \; + \; B.$$

Numerous experimental determinations of the constants A and B provide $A \; = \; 2.44$ and $B = 5.2$ within a 5% error (Pope, 2000). Tradition has it to write the function as:

$$u(z) \; = \; \frac{u_*}{\mathcal{K}} \, \ln \frac{u_* z}{\nu} \; + \; 5.2 \, u_*, \tag{8.4}$$

where $\mathcal{K} = 1/A = 0.41$ is called the *von Kármán constant*[1]

The portion of the curve closer to the wall, where the logarithmic law fails, may be approximated by the laminar solution. Constant laminar stress $\nu du/dz = \tau_b/\rho = u_*^2$ implies $u(z) = u_*^2 z/\nu$ there. Ignoring the region of transition in which the velocity profile gradually

---

[1]in honor of Theodore von Kármán (1881–1963), Hungarian-born physicist and engineer who made significant contributions to fluid mechanics while working in Germany and who first introduced this notation.
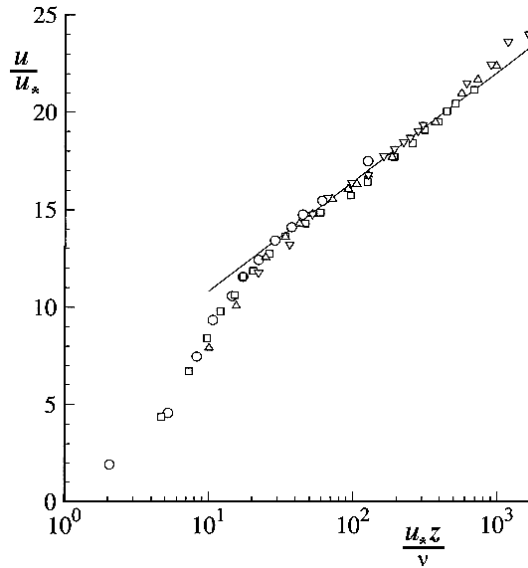
Figure 8-1 Mean velocity profiles in fully developed turbulent channel flow measured by Wei and Willmarth (1989) at various Reynolds numbers: circles Re = 2970, squares Re = 14914, up-right triangles Re = 22776, and down-right triangles Re = 39582. The straight line on this log-linear plot corresponds to the logarithmic profile of Equation (8.2). (From Pope, 2000)

changes from one solution to the other, we can attempt to connect the two. Doing so yields $u_*z/\nu = 11$. This sets the thickness of the laminar boundary layer δ as the value of z for which $u_*z/\nu = 11$, *i.e.*,

$$\delta \;=\; 11\,\frac{\nu}{u_*}\;. \tag{8.5}$$

Most textbooks (*e.g.*, Kundu, 1990) give $\delta = 5\nu/u_*$, for the region in which the velocity profile is strictly laminar, and label the region between $5\nu/u_*$ and $30\nu/u_*$ as the *buffer layer*, the transition zone between laminar and fully turbulent flow.

For water in ambient conditions, the molecular viscosity ν is equal to 1.0×10^{-6} m^2/s, while the friction velocity in the ocean rarely falls below 1 mm/s. This implies that δ hardly exceeds a centimeter in the ocean and is almost always smaller than the height of the cobbles, ripples and other asperities that typically line the bottom of the ocean basin. Similarly for the atmosphere: the air viscosity at ambient temperature and pressure is about 1.5×10^{-5} m^2/s and u_* rarely falls below 1 cm/s, giving $\delta < 5$ cm, smaller than most irregularities on land and wave heights at sea.

When this is the case, the velocity profile above the bottom asperities no longer depends on the molecular viscosity of the fluid but on the so-called *roughness height* z_0, such that

$$u(z) \;=\; \frac{u_*}{\mathcal{K}}\,\ln\,\frac{z}{z_0}\;, \tag{8.6}$$

as depicted in Figure 8-2. It is important to note that the roughness height is not the average height of bumps on the surface but is a small fraction of it, about one tenth (Garratt, 1992, page 87).
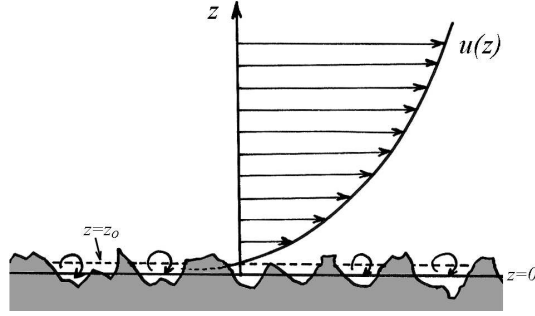
Figure 8-2 Velocity profile in the vicinity of a rough wall. The roughness heigh z_0 is smaller than the averaged height of the surface asperities. So, the velocity u falls to zero somewhere within the asperities, where local flow degenerates into small vortices between the peaks, and the negative values predicted by the logarithmic profile are not physically realized.

8.1.2 Eddy viscosity

We have already mentioned in Section 5.2 what an eddy diffusivity or viscosity is and how it can be formulated in the case of a homogeneous turbulence field, *i.e.*, away from boundaries. Near a boundary, the turbulence ceases to be isotropic and an alternate formulation needs to be developed.

In analogy with Newton's law for viscous fluids, which has the tangential stress τ proportional to the velocity shear du/dz with the coefficient of proportionality being the molecular viscosity ν, we write for turbulent flow:

$$\tau = \rho_0 \nu_E \frac{du}{dz}, \tag{8.7}$$

where the turbulent viscosity ν_E supersedes the molecular viscosity ν. For the logarithmic profile (8.6) of a flow along a rough surface, the velocity shear is $du/dz = u_*/\mathcal{K}z$ and the stress τ is uniform across the flow (at least in the vicinity of the boundary for lack of other significant forces): $\tau = \tau_b = \rho u_*^2$, giving

$$\rho_0 u_*^2 = \rho_0 \nu_E \frac{u_*}{\mathcal{K}z}$$

and thus

$$\nu_E = \mathcal{K}z u_*. \tag{8.8}$$

Note that unlike the molecular viscosity, the turbulent viscosity is not constant in space, for it is not a property of the fluid but of the flow, including its geometry. From its dimension ($[\nu_E] = L^2 T^{-1}$), we verify that (8.8) is dimensionally correct and note that it can be expressed as the product of a length by the friction velocity

$$\nu_E = l_m u_*, \tag{8.9}$$

with the *mixing length* l_m defined as

$$l_m = \mathcal{K}z. \tag{8.10}$$

This parameterization is occasionally used for cases other than boundary layers (see Chapter 14).

The preceding considerations ignored the effect of rotation. When rotation is present, the character of the boundary layer changes dramatically.

8.2 Friction and rotation

After the development of the equations governing geophysical motions (Sections 4.1 to 4.4), a scale analysis was performed to evaluate the relative importance of the various terms (Section 4.5). In the horizontal momentum equations [(4.21a) and (4.21b)], each term was compared to the Coriolis term, and a corresponding dimensionless ratio was defined. For vertical friction, the dimensionless ratio was the *Ekman number*:

$$Ek = \frac{\nu_E}{\Omega H^2},$$ (8.11)

where ν_E is the eddy viscosity, Ω the ambient rotation rate, and H the height (depth) scale of the motion (the total thickness if the fluid is homogeneous).

Typical geophysical flows, as well as laboratory experiments, are characterized by very small Ekman numbers. For example, in the ocean at midlatitudes ($\Omega \simeq 10^{-4}$ s^{-1}), motions modeled with an eddy-intensified viscosity $\nu_E = 10^{-2}$ m^2/s (much larger than the molecular viscosity of water, equal to 1.0×10^{-6} m^2/s) and extending over a depth of about 1000 m have an Ekman number of about 10^{-4}.

The smallness of the Ekman number indicates that vertical friction plays a very minor role in the balance of forces and may, consequently, be omitted from the equations. This is usually done and with great success. However, something is then lost. The frictional terms happen to be those with the highest order of derivatives among all terms of the momentum equations. Thus, when friction is neglected, the order of the set of differential equations is reduced, and not all boundary conditions can be applied simultaneously. Usually, slipping along the bottom must be accepted.

Since Ludwig Prandtl[2] and his general theory of boundary layers, we know that in such a circumstance the fluid system exhibits two distinct behaviors: At some distance from the boundaries, in what is called the *interior*, friction is usually negligible, whereas, near a boundary (wall) and across a short distance, called the *boundary layer*, friction acts to bring the finite interior velocity to zero at the wall.

The thickness, d, of this thin layer is such that the Ekman number is on the order of one at that scale, allowing friction to be a dominant force:

$$\frac{\nu_E}{\Omega d^2} \sim 1,$$

which leads to

$$d \sim \sqrt{\frac{\nu_E}{\Omega}} \, .$$ (8.12)

---

[2]See biography at the end of this chapter.

Obviously, d is much less than H, and the boundary layer occupies a very small portion of the flow domain. For the oceanic values cited above ($\nu_E = 10^{-2}$ m²/s and $\Omega = 10^{-4}$ s^{-1}), d is about 10 m.

Because of the Coriolis effect, the frictional boundary layer of geophysical flows, called the *Ekman layer*, differs greatly from the boundary layer in nonrotating fluids. Although, the traditional boundary layer has no particular thickness and grows either downstream or with time, the existence of the depth scale d in rotating fluids suggests that the Ekman layer can be characterized by a fixed thickness. [Note that as the rotational effects disappear ($\Omega \rightarrow 0$), d tends to infinity, exemplifying this essential difference between rotating and nonrotating fluids.]

8.3   The bottom Ekman layer

Let us consider a uniform, geostrophic flow in a homogeneous fluid over a flat bottom (Figure 8-3). This bottom exerts a frictional stress against the flow, bringing the velocity gradually to zero within a thin layer above the bottom. We now solve for the structure of this layer.
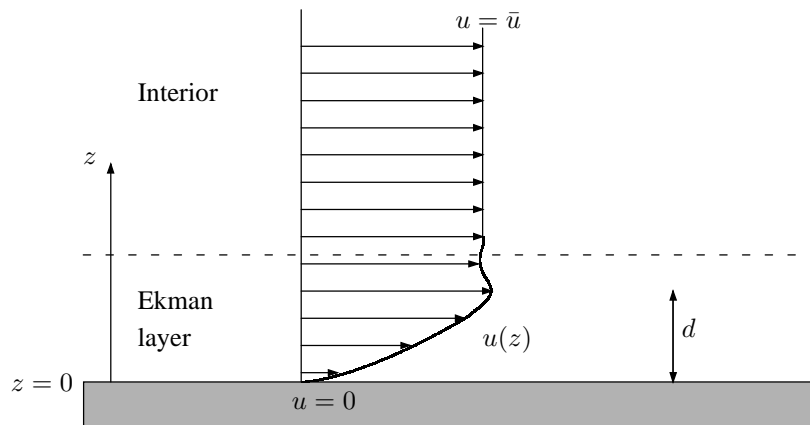

Figure 8-3 Frictional influence of a flat bottom on a uniform flow in a rotating framework.

In the absence of horizontal gradients (the interior flow is said to be uniform) and of temporal variations, continuity equation (4.21d) yields $\partial w/\partial z = 0$ and thus $w = 0$ in the thin layer near the bottom. The remaining equations are the following reduced forms of

(4.21a) through (4.21c):

$$- fv = - \frac{1}{\rho_0} \frac{\partial p}{\partial x} + \nu_E \frac{\partial^2 u}{\partial z^2} \tag{8.13a}$$

$$+ fu = - \frac{1}{\rho_0} \frac{\partial p}{\partial y} + \nu_E \frac{\partial^2 v}{\partial z^2} \tag{8.13b}$$

$$0 = - \frac{1}{\rho_0} \frac{\partial p}{\partial z}, \tag{8.13c}$$

where f is the Coriolis parameter (taken as a constant here), ρ_0 is the fluid density, and ν_E is the eddy viscosity (taken as a constant for simplicity). The horizontal gradient of the pressure p is retained because a uniform flow requires a uniformly varying pressure (Section 7.1). For convenience, we align the x–axis with the direction of the interior flow, which is of velocity $\bar{u}$. The boundary conditions are then

$$\text{Bottom } (z = 0): \quad u = 0, \quad v = 0, \tag{8.14a}$$
$$\text{Toward the interior } (z \gg d): \quad u = \bar{u}, \quad v = 0, \quad p = \bar{p}(x, y). \tag{8.14b}$$

By virtue of equation (8.13c), the dynamic pressure p is the same at all depths; thus, $p = \bar{p}(x, y)$ in the outer flow as well as throughout the boundary layer. In the outer flow ($z \gg d$, mathematically equivalent to $z \to \infty$), equations (8.13a) and (8.13b) relate the velocity to the pressure gradient:

$$0 = - \frac{1}{\rho_0} \frac{\partial \bar{p}}{\partial x},$$
$$f\bar{u} = - \frac{1}{\rho_0} \frac{\partial \bar{p}}{\partial y} = \text{constant.}$$

Substitution of these derivatives in the same equations, which are now taken at any depth, yields

$$- fv = \nu_E \frac{d^2 u}{dz^2} \tag{8.15a}$$

$$f (u - \bar{u}) = \nu_E \frac{d^2 v}{dz^2}. \tag{8.15b}$$

Seeking a solution of the type $u = \bar{u} + A \exp(\lambda z)$ and $v = B \exp(\lambda z)$, we find that λ obeys $\nu^2 \lambda^4 + f^2 = 0$; that is,

$$\lambda = \pm (1 \pm i) \frac{1}{d}$$

where the distance d is defined by

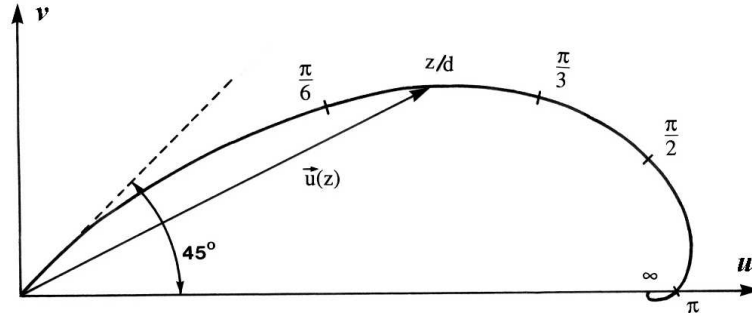$$d = \sqrt{\frac{2\nu_E}{f}}. \tag{8.16}$$

Figure 8-4   The velocity spiral in the bottom Ekman layer. The figure is drawn for the Northern Hemisphere ($f > 0$), and the deflection is to the left of the current above the layer. The reverse holds for the Southern Hemisphere.

Here, we have restricted ourselves to cases with positive f (Northern Hemisphere). Note the similarity to (8.12). Boundary conditions (8.14b) rule out the exponentially growing solutions, leaving

$$u = \bar{u} + e^{-z/d} \left(A \cos \frac{z}{d} + B \sin \frac{z}{d} \right) \tag{8.17a}$$

$$v = e^{-z/d} \left(B \cos \frac{z}{d} - A \sin \frac{z}{d} \right), \tag{8.17b}$$

and the application of the remaining boundary conditions (8.14a) yields $A = -\bar{u}$, $B = 0$, or

$$u = \bar{u} \left(1 - e^{-z/d} \cos \frac{z}{d} \right) \tag{8.18a}$$

$$v = \bar{u}\, e^{-z/d} \sin \frac{z}{d} . \tag{8.18b}$$

This solution has a number of important properties. First and foremost, we notice that the distance over which it approaches the interior solution is on the order of d. Thus, expression (8.16) gives the thickness of the boundary layer. For this reason, d is called the *Ekman depth*. A comparison with (8.12) confirms the earlier argument that the boundary-layer thickness is the one corresponding to a local Ekman number near unity.

The preceding solution also tells us that there is, in the boundary layer, a flow transverse to the interior flow ($v \neq 0$). Very near the bottom ($z \to 0$), this component is equal to the downstream velocity ($u \sim v \sim \bar{u}z/d$), thus implying that the near-bottom velocity is at 45 degrees to the left of the interior velocity (Figure 8-4). (The boundary flow is to the right of the interior flow for $f < 0$.) Further up, where u reaches a first maximum ($z = 3\pi d/4$), the velocity in the direction of the flow is greater than in the interior ($u = 1.07\bar{u}$). (Viscosity can occasionally fool us!)

It is instructive to calculate the net transport of fluid transverse to the main flow:

$$\mathrm{V} = \int_0^\infty v\, dz = \frac{\bar{u}d}{2} , \tag{8.19}$$

which is proportional to the interior velocity and the Ekman depth.

8.4 Generalization to non-uniform currents

Let us now consider a more complex interior flow, namely, a spatially nonuniform flow that is varying on a scale sufficiently large to be in geostrophic equilibrium (low Rossby number, as in Section 7.1). Thus,

$$- f\bar{v} \;=\; - \frac{1}{\rho_0} \frac{\partial \bar{p}}{\partial x} \,, \quad f\bar{u} \;=\; - \frac{1}{\rho_0} \frac{\partial \bar{p}}{\partial y} \,,$$

where the pressure $\bar{p}(x, y, t)$ is arbitrary. For a constant Coriolis parameter, this flow is non-divergent ($\partial\bar{u}/\partial x + \partial\bar{v}/\partial y = 0$). The boundary-layer equations are now

$$- f(v - \bar{v}) \;=\; \nu_E \frac{\partial^2 u}{\partial z^2} \tag{8.20a}$$

$$f(u - \bar{u}) \;=\; \nu_E \frac{\partial^2 v}{\partial z^2} \,, \tag{8.20b}$$

and the solution that satisfies the boundary conditions aloft ($u \to \bar{u}$ and $v \to \bar{v}$ for $z \to \infty$) is

$$u \;=\; \bar{u} \,+\, e^{-z/d} \left(A \cos\frac{z}{d} \,+\, B \sin\frac{z}{d} \right) \tag{8.21}$$

$$v \;=\; \bar{v} \,+\, e^{-z/d} \left(B \cos\frac{z}{d} \,-\, A \sin\frac{z}{d} \right). \tag{8.22}$$

Here, the "constants" of integration A and B are independent of z but, in general, dependent on x and y through $\bar{u}$ and $\bar{v}$. Imposing $u = v = 0$ along the bottom ($z = 0$) sets their values, and the solution is:

$$u \;=\; \bar{u} \left(1 - e^{-z/d} \cos\frac{z}{d} \right) \,-\, \bar{v} \, e^{-z/d} \sin\frac{z}{d} \tag{8.23a}$$

$$v \;=\; \bar{u} \, e^{-z/d} \sin\frac{z}{d} \,+\, \bar{v} \left(1 - e^{-z/d} \cos\frac{z}{d} \right). \tag{8.23b}$$

The transport attributed to the boundary-layer structure has components given by

$$\mathrm{U} \;=\; \int_0^\infty (u - \bar{u}) \, dz \;=\; - \frac{d}{2} \, (\bar{u} + \bar{v}) \tag{8.24a}$$

$$\mathrm{V} \;=\; \int_0^\infty (v - \bar{v}) \, dz \;=\; \frac{d}{2} \, (\bar{u} - \bar{v}). \tag{8.24b}$$
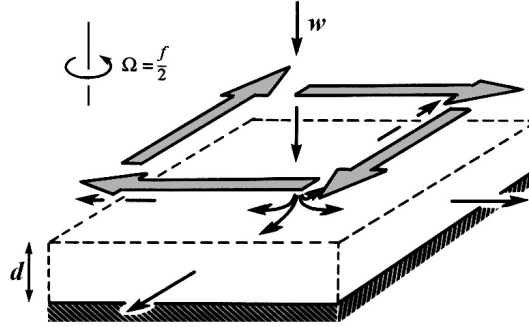
Figure 8-5 Divergence in the bottom Ekman layer and compensating downwelling in the interior. Such a situation arises in the presence of an anticyclonic gyre in the interior, as depicted by the large horizontal arrows. Similarly, interior cyclonic motion causes convergence in the Ekman layer and upwelling in the interior.

Since this transport is not necessarily parallel to the interior flow, it is likely to have a non-zero divergence. Indeed,

$$
\frac{\partial U}{\partial x} + \frac{\partial V}{\partial y} = \int_0^\infty \left(\frac{\partial u}{\partial x} + \frac{\partial v}{\partial y} \right) dz = -\frac{d}{2} \left(\frac{\partial \bar{v}}{\partial x} - \frac{\partial \bar{u}}{\partial y} \right)
$$
$$
= -\frac{d}{2\rho_0 f} \nabla^2 \bar{p}. \tag{8.25}
$$

The flow in the boundary layer converges or diverges if the interior flow has a relative vorticity. The situation is depicted in Figure 8-5. The question is: From where does the fluid come, or where does it go, to meet this convergence or divergence? Because of the presence of a solid bottom, the only possibility is that it be supplied from the interior by means of a vertical velocity. But, remember (Section 7.1) that geostrophic flows must be characterized by

$$
\frac{\partial \bar{w}}{\partial z} = 0, \tag{8.26}
$$

that is, the vertical velocity must occur throughout the depth of the fluid. Of course, since the divergence of the flow in the Ekman layer is proportional to the Ekman depth, d, which is very small, this vertical velocity is weak.

The vertical velocity in the interior, called *Ekman pumping*, can be evaluated by a vertical integration of the continuity equation (4.21d), using $w(z = 0) = 0$ and $w(z \to \infty) = \bar{w}$:

$$
\bar{w} = -\int_0^\infty \left(\frac{\partial u}{\partial x} + \frac{\partial v}{\partial y} \right) dz = \frac{d}{2} \left(\frac{\partial \bar{v}}{\partial x} - \frac{\partial \bar{u}}{\partial y} \right)
$$
$$
= \frac{d}{2\rho_0 f} \nabla^2 \bar{p} = \frac{1}{\rho_0} \sqrt{\frac{\nu_E}{2f^3}} \nabla^2 \bar{p}. \tag{8.27}
$$

So, the greater the vorticity of the mean flow, the greater the upwelling/downwelling. Also, the effect increases toward the equator (decreasing $f = 2\Omega \sin \varphi$ and increasing d). The direction of the vertical velocity is upward in a cyclonic flow (counterclockwise in the Northern Hemisphere) and downward in an anticyclonic flow (clockwise in the Northern Hemisphere).

In the Southern Hemisphere, where $f < 0$, the Ekman layer thickness d must be redefined with the absolute value of f: $d = \sqrt{2\nu_E/|f|}$, but the previous rule remains: the vertical velocity is upward in a cyclonic flow and downward in an anticyclonic flow. The difference is that cyclonic flow is clockwise and anticyclonic flow is counterclockwise.

8.5   The Ekman layer over uneven terrain

It is noteworthy to explore how an irregular topography may affect the structure of the Ekman layer and, in particular, the magnitude of the vertical velocity in the interior. For this, consider a horizontal geostrophic interior flow $(\bar{u}, \bar{v})$, not necessarily spatially uniform, over an uneven terrain of elevation $z = b(x, y)$ above a horizontal reference level. To be faithful to our restriction (Section 4.3) to geophysical flows much wider than they are thick, we shall assume that the bottom slope $(\partial b/\partial x, \partial b/\partial y)$ is everywhere small ($\ll 1$). This is hardly a restriction in most atmospheric and oceanic situations.

Our governing equations are again (8.20), coupled to the continuity equation (4.21d), but the boundary conditions are now

$$\text{Bottom } (z = b): \quad u = 0, \;\; v = 0, \;\; w = 0, \quad\quad (8.28)$$

$$\text{Toward the interior } (z \gg d): \quad u = \bar{u}, \;\; v = \bar{v}. \quad\quad (8.29)$$

The solution is the previous solution (8.23) with z replaced by $z - b$:

$$u = \bar{u} - e^{(b-z)/d} \left(\bar{u} \, \cos \frac{z-b}{d} \;+\; \bar{v} \, \sin \frac{z-b}{d} \right) \quad\quad (8.30a)$$

$$v = \bar{v} + e^{(b-z)/d} \left(\bar{u} \, \sin \frac{z-b}{d} \;-\; \bar{v} \, \cos \frac{z-b}{d} \right). \quad\quad (8.30b)$$

We note that the vertical thickness of the boundary layer is still measured by $d = \sqrt{2\nu_E/f}$. However, the boundary layer is now oblique, and its true thickness, measured perpendicularly to the bottom, is slightly reduced by the cosine of the small bottom slope.

The vertical velocity is then determined from the continuity equation:

$$\frac{\partial w}{\partial z} = -\frac{\partial u}{\partial x} - \frac{\partial v}{\partial y}$$

$$= e^{(b-z)/d} \left\{ \left(\frac{\partial \bar{v}}{\partial x} - \frac{\partial \bar{u}}{\partial y} \right) \sin \frac{z-b}{d} \right.$$

$$+ \frac{1}{d} \frac{\partial b}{\partial x} \left[(\bar{u} - \bar{v}) \cos \frac{z-b}{d} + (\bar{u} + \bar{v}) \sin \frac{z-b}{d} \right]$$

$$\left. + \frac{1}{d} \frac{\partial b}{\partial y} \left[(\bar{u} + \bar{v}) \cos \frac{z-b}{d} - (\bar{u} - \bar{v}) \sin \frac{z-b}{d} \right] \right\},$$

where use has been made of the fact that the interior geostrophic flow has no divergence ($\partial \bar{u}/\partial x + \partial \bar{v}/\partial y = 0$). A vertical integration from the bottom ($z = b$), where the vertical velocity vanishes ($w = 0$ because u and v are also zero there) into the interior ($z \to +\infty$) where the vertical velocity assumes a vertically uniform value ($w = \bar{w}$), yields

$$\bar{w} = \left(\bar{u} \frac{\partial b}{\partial x} + \bar{v} \frac{\partial b}{\partial y} \right) + \frac{d}{2} \left(\frac{\partial \bar{v}}{\partial x} - \frac{\partial \bar{u}}{\partial y} \right). \tag{8.31}$$

The interior vertical velocity thus consists of two parts: a component that ensures no normal flow to the bottom [see (7.10)] and an Ekman-pumping contribution, as if the bottom were horizontally flat [see (8.27)].

The vanishing of the flow component perpendicular to the bottom must be met by the inviscid dynamics of the interior, giving rise to the first contribution to $\bar{w}$. The role of the boundary layer is to bring the tangential velocity to zero at the bottom. This explains the second contribution to $\bar{w}$. Note that the Ekman pumping is not affected by the bottom slope.

The preceding solution can also be applied to the lower portion of the atmospheric boundary layer. This was first done by Akerblom (1908), and matching between the logarithmic layer close to the ground (Section 8.1.1) with the Ekman layer further aloft was performed by Van Dyke (1975). Oftentimes, however, the lower atmosphere is in a stable (stratified) or unstable (convecting) state, and the neutral state during which Ekman dynamics prevail is more the exception than the rule.

8.6   The surface Ekman layer

An Ekman layer occurs not only along bottom surfaces but wherever there is a horizontal frictional stress. This is the case, for example, along the ocean surface, where waters are subject to a wind stress. In fact, this is precisely the situation first examined by Vagn Walfrid Ekman[3]. Fridtjof Nansen[4] had noticed during his cruises to northern latitudes that icebergs drift not downwind but systematically at some angle to the right of the wind. Ekman, his student at the time, reasoned that the cause of this bias was the earth's rotation and subsequently developed the mathematical representation that now bears his name. The solution

---

[3]See biography at the end of this chapter.
[4]Fridtjof Nansen (1861–1930), Norwegian oceanographer famous for his Arctic expeditions and Nobel Peace Prize laureate (1922).

was originally published in his 1902 doctoral thesis and again, in a more complete article, three years later (Ekman, 1905). In a subsequent article (Ekman, 1906), he mentioned the relevance of his theory to the lower atmosphere, where the wind approaches a geostrophic value with increasing height.
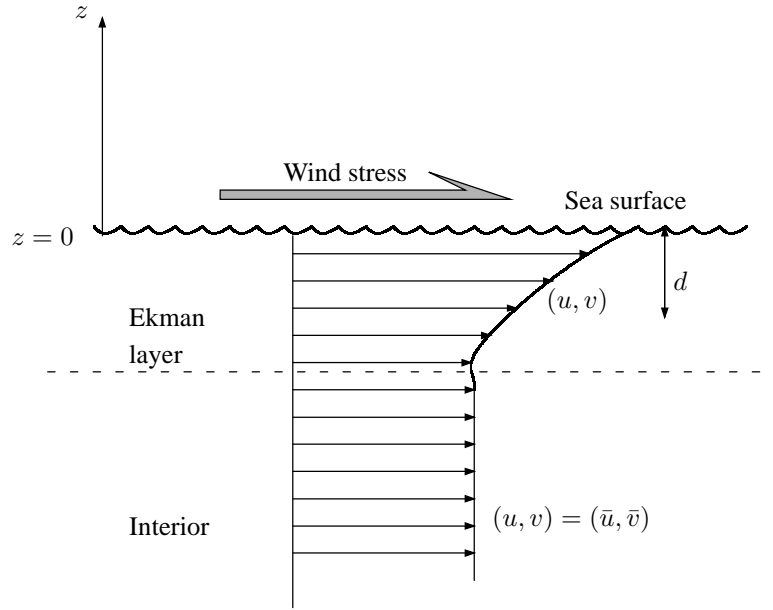

Figure 8-6 The surface Ekman layer generated by a wind stress on the ocean.

Let us consider the situation depicted in Figure 8-6, where an ocean region with interior flow field $(\bar{u}, \bar{v})$ is subjected to a wind stress (τ^x, τ^y) along its surface. Again, assuming steady conditions, a homogeneous fluid, and a geostrophic interior, we obtain the following equations and boundary conditions for the flow field (u, v) in the surface Ekman layer:

$$- f\,(v - \bar{v}) \;=\; \nu_E\,\frac{\partial^2 u}{\partial z^2} \tag{8.32a}$$

$$+ f\,(u - \bar{u}) \;=\; \nu_E\,\frac{\partial^2 v}{\partial z^2} \tag{8.32b}$$

$$\text{Surface } (z = 0): \quad \rho_0\nu_E\frac{\partial u}{\partial z} = \tau^x, \;\; \rho_0\nu_E\frac{\partial v}{\partial z} = \tau^y \tag{8.32c}$$

$$\text{Toward interior } (z \rightarrow -\infty): \quad u = \bar{u}, \;\; v = \bar{v}. \tag{8.32d}$$
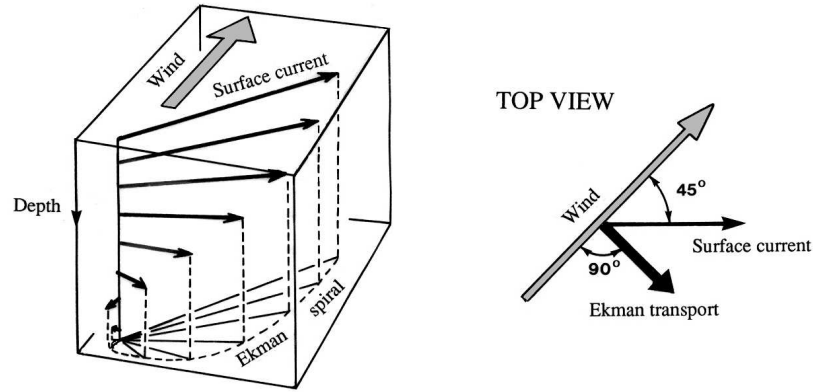
Figure 8-7 Structure of the surface Ekman layer. The figure is drawn for the Northern Hemisphere ($f > 0$), and the deflection is to the right of the surface stress. The reverse holds for the Southern Hemisphere.

The solution to this problem is

$$u = \bar{u} + \frac{\sqrt{2}}{\rho_0 f d} e^{z/d} \left[\tau^x \cos\left(\frac{z}{d} - \frac{\pi}{4}\right) - \tau^y \sin\left(\frac{z}{d} - \frac{\pi}{4}\right) \right] \qquad (8.33a)$$

$$v = \bar{v} + \frac{\sqrt{2}}{\rho_0 f d} e^{z/d} \left[\tau^x \sin\left(\frac{z}{d} - \frac{\pi}{4}\right) + \tau^y \cos\left(\frac{z}{d} - \frac{\pi}{4}\right) \right], \qquad (8.33b)$$

in which we note that the departure from the interior flow $(\bar{u}, \bar{v})$ is exclusively due to the wind stress. In other words, it does not depend on the interior flow. Moreover, this wind-driven flow component is inversely proportional to the Ekman-layer depth, d, and may be very large. Physically, if the fluid is almost inviscid (small ν, hence short d), a moderate surface stress can generate large drift velocities.

The wind-driven horizontal transport in the surface Ekman layer has components given by

$$U = \int_{-\infty}^{0} (u - \bar{u}) \, dz = \frac{1}{\rho_0 f} \tau^y \qquad (8.34a)$$

$$V = \int_{-\infty}^{0} (v - \bar{v}) \, dz = \frac{-1}{\rho_0 f} \tau^x. \qquad (8.34b)$$

Surprisingly, it is oriented perpendicular to the wind stress (Figure 8-7), to the right in the Northern Hemisphere and to the left in the Southern Hemisphere. This fact explains why icebergs, which float mostly underwater, systematically drift to the right of the wind in the North Atlantic, as observed by Fridtjof Nansen.
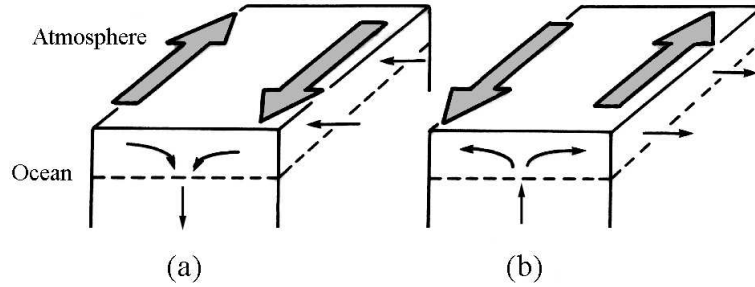
Figure 8-8 Ekman pumping in an ocean subject to sheared winds (case of Northern Hemisphere).

As for the bottom Ekman layer, let us determine the divergence of the flow, integrated over the boundary layer:

$$\int_{-\infty}^{0} \left(\frac{\partial u}{\partial x} + \frac{\partial v}{\partial y} \right) dz = \frac{1}{\rho_0} \left[\frac{\partial}{\partial x} \left(\frac{\tau^y}{f} \right) - \frac{\partial}{\partial y} \left(\frac{\tau^x}{f} \right) \right]. \tag{8.35}$$

At constant f, the contribution is entirely due to the wind stress since the interior geostrophic flow is nondivergent. It is proportional to the wind-stress curl and, most importantly, it is independent of the value of the viscosity. It can be shown furthermore that this property continues to hold even when the turbulent eddy viscosity varies spatially (see Analytical Problem 8-7).

If the wind stress has a non-zero curl, the divergence of the Ekman transport must be provided by a vertical velocity throughout the interior. A vertical integration of the continuity equation, (4.21d), across the Ekman layer with $w(z = 0)$ and $w(z \rightarrow -\infty) = \bar{w}$ yields

$$\begin{aligned} \bar{w} &= + \int_{-\infty}^{0} \left(\frac{\partial u}{\partial x} + \frac{\partial v}{\partial y} \right) dz \\ &= \frac{1}{\rho_0} \left[\frac{\partial}{\partial x} \left(\frac{\tau^y}{f} \right) - \frac{\partial}{\partial y} \left(\frac{\tau^x}{f} \right) \right] = w_{\text{Ek}}. \end{aligned} \tag{8.36}$$

This vertical velocity is called *Ekman pumping*. In the Northern Hemisphere ($f > 0$), a clockwise wind pattern (negative curl) generates a downwelling (Figure 8-8a), whereas a counterclockwise wind pattern causes upwelling (Figure 8-8b). The directions are opposite in the Southern Hemisphere. Ekman pumping is a very effective mechanism by which winds drive subsurface ocean currents (Pedlosky, 1996; see also Chapter 20).

8.7 The Ekman layer in real geophysical flows

The preceding models of bottom and surface Ekman layers are highly idealized, and we do not expect their solutions to match actual atmospheric and oceanic observations closely
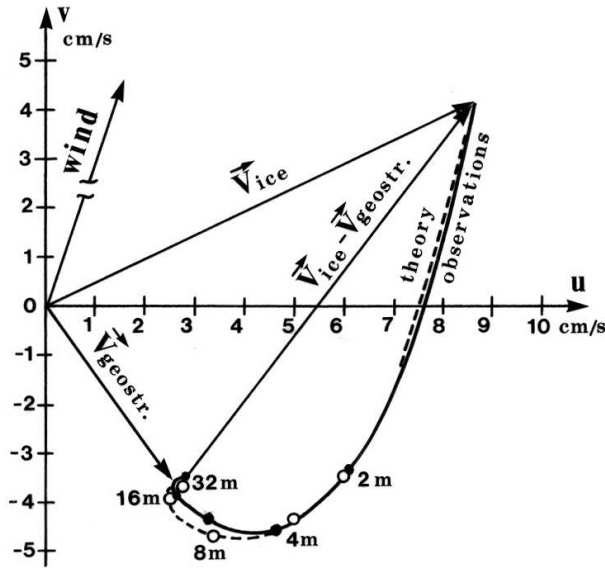
Figure 8-9 Comparison between observed currents below a drifting ice floe at 84.3°N and theoretical predictions based on an eddy viscosity $\nu_E = 2.4 \times 10^{-3}$ m²/s. (Reprinted from *Deep-Sea Research*, 13, Kenneth Hunkins, Ekman drift currents in the Arctic Ocean, p. 614, ©1966, with kind permission from Pergamon Press Ltd, Headington Hill Hall, Oxford 0X3 0BW, UK)

(except in some cases; see Figure 8-9). Two factors, among others, account for substantial differences: turbulence and stratification.

It was noted at the end of Chapter 4 that geophysical flows have large Reynolds numbers and are therefore in a state of turbulence. Replacing the molecular viscosity of the fluid by a much greater eddy viscosity, as performed in Section 4.2, is a first attempt to recognize the enhanced transfer of momentum in a turbulent flow. However, in a shear flow such as in an Ekman layer, the turbulence is not homogeneous, being more vigorous where the shear is greater and also partially suppressed in the proximity of the boundary where the size of turbulent eddies is restricted. In the absence of an exact theory of turbulence, several schemes have been proposed. At a minimum, the eddy viscosity should be made to vary in the vertical (Madsen, 1977) and should be a function of the bottom stress value (Cushman-Roisin and Malačič, 1997). A number of schemes have been proposed (see Section 4.2), with varying degrees of success. Despite numerous disagreements among models and with field observations, two results nonetheless stand out as quite general. The first is that the angle between the near-boundary velocity and that in the interior or that of the surface stress (depending on the type of Ekman layer) is always substantially less than the theoretical value of 45° and is found to range between 5° and 20° (Figure 8-10). See also Stacey *et al.* (1986).

The second result is a formula for the vertical scale of the Ekman-layer thickness:

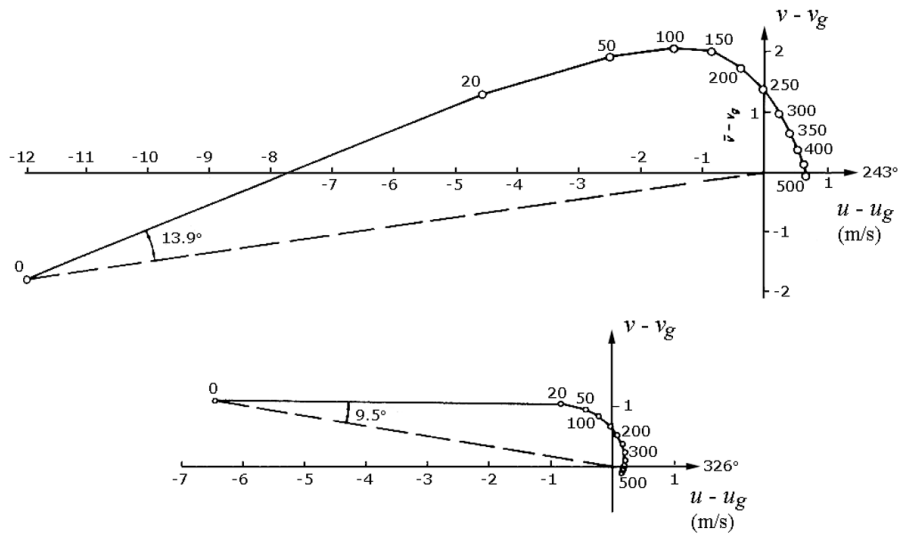$$d \simeq 0.4 \frac{u_*}{f}, \tag{8.37}$$

Figure 8-10 Wind vectors minus geostrophic wind as a function of height (in meters) in the maritime friction layer near the Scilly Isles. *Top diagram*: Case of warm air over cold water. *Bottom diagram*: Case of cold air over warm water. (Adapted from Roll, 1965)

where u_* is the turbulent friction velocity defined in (8.1). The numerical factor is derived from observations (Garratt, 1992, Appendix 3). Whereas 0.4 is the most commonly accepted value, there is evidence that certain oceanic conditions call for a somewhat smaller value (Mofjeld and Lavelle, 1984; Stigebrandt, 1985).

Taking u_* as the turbulent velocity and the (unknown) Ekman-layer depth scale, d, as the size of the largest turbulent eddies, we write

$$\nu_E \sim u_* d. \tag{8.38}$$

Then, using rule 8.12 to determine the boundary-layer thickness, we obtain

$$1 \sim \frac{\nu_E}{fd^2} \sim \frac{u_*}{fd},$$

which immediately leads to (8.37).

The other major element missing from the Ekman-layer formulations of the previous sections is the presence of vertical density stratification. Although the effects of stratification are not discussed in detail until Chapter 11, it can be anticipated here that the gradual change of density with height (lighter fluid above heavier fluid) hinders vertical movements, thereby reducing vertical mixing of momentum by turbulence; it also allows the motions at separate levels to act less coherently and to generate internal gravity waves. As a consequence, stratification reduces the thickness of the Ekman layer and increases the veering of the velocity vector with height (Garratt, 1992, Section 6.2). For a study of the oceanic wind-driven Ekman

layer in the presence of density stratification, the reader is referred to Price and Sundermeyer (1999).

The surface atmospheric layer during daytime over land and above warm currents at sea is frequently in a state of convection because of heating from below. In such situations, the Ekman dynamics give way to convective motions, and a controlling factor, besides the geostrophic wind aloft, is the intensity of the surface heat flux. An elementary model is presented later (Section 14.7). Because Ekman dynamics then play a secondary role, the layer is simply called the *atmospheric boundary layer*. The interested reader is referred to books on the subject by Stull (1988), Sorbjan (1989), Zilitinkevich (1991) or Garratt (1992).

8.8   Numerical simulation of shallow flows

The theory presented up to now largely relies on the assumption of a constant turbulent viscosity. For real flows, however, turbulence is rarely uniform, and eddy-diffusion profiles must be considered. Such complexity renders the analytical treatment tedious or even impossible, and numerical methods need to be employed.
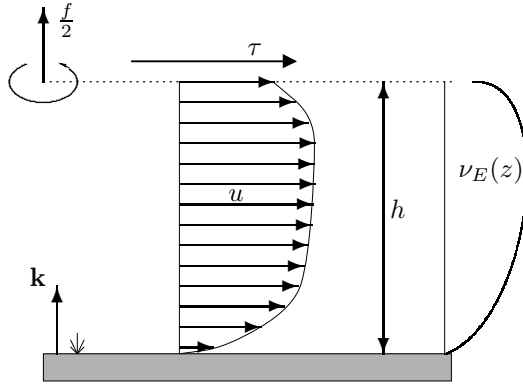

Figure 8-11 A vertically confined fluid flow, with bottom and top Ekman layers bracketing a non-uniform velocity profile. The vertical structure can be calculated by a one-dimensional model spanning the entire fluid column even-though the turbulent viscosity $\nu_E(z)$ may vary in the vertical.

To illustrate the approach, we reinstate non-stationary terms and assume a vertically varying eddy-viscosity (Figure 8-11) but retain the hydrostatic approximation (8.13c) and continue to consider a fluid of homogeneous density. The governing equations for u and v are

$$\frac{\partial u}{\partial t} - fv = -\frac{1}{\rho_0}\frac{\partial p}{\partial x} + \frac{\partial}{\partial z}\left(\nu_E(z)\frac{\partial u}{\partial z}\right) \tag{8.39a}$$

$$\frac{\partial v}{\partial t} + fu = -\frac{1}{\rho_0}\frac{\partial p}{\partial y} + \frac{\partial}{\partial z}\left(\nu_E(z)\frac{\partial v}{\partial z}\right) \tag{8.39b}$$

$$0 = -\frac{1}{\rho_0}\frac{\partial p}{\partial z}. \tag{8.39c}$$

From the last equation it is clear that the horizontal pressure gradient is independent of z.